Congenital Heart Disease

17

Priya Pillutla and Jamil A. Aboulhosn

Congenital heart disease (CHD) represents a heterogeneous group of disorders characterized by cardiovascular anomalies that are present from birth. These abnormalities vary from simple isolated lesions such as an isolated bicuspid aortic valve to complex syndromes characterized by multiple cardiovascular abnormalities, such as Noonan's syndrome. The clinician treating patients with CHD takes on a daunting task because they must fully understand not only the anatomy and hemodynamics of the "normal" cardiovascular system but also the perturbations present in patients with a wide mix of unoperated and post-operative congenital cardiovascular defects. Added is the burden of calculating the effects of acquired diseases that develop in a growing, aging CHD population.

Cross-sectional diagnostic imaging modalities such as MRI and CT allow for excellent visualization of intracardiac and extracardiac anatomy and complement the traditional diagnostic tools such as echocardiography and cardiac catheterization. Advances in technology have improved temporal and spatial resolution and now enable CT to be used as an accurate noninvasive clinical instrument that is fast replacing invasive cineangiography in the evaluation of CHD. In fact, CT imaging has become a routinely used tool when detailed morphologic assessment of complex anatomy is required. The strength of CT rests in the capacity of ECG-gated multidetector scanners to provide submillimeter angiographic images of stunning clarity. Moreover, cardiac CT may be utilized when MRI is contraindicated, such as in patients who are pacemaker-dependent. CT is also less prone to artifacts from metallic stents or devices, which are widely utilized in patients with both operated and unoperated CHD. The high negative predictive value of cardiac CT in the evaluation of coronary artery disease has made it an ideal screening tool before cardiac surgery in the adult CHD patient.

This chapter focuses on the use of CT angiography in patients with CHD and the complementary role that it plays in the management of this complex subset of patients (Figs. 17.1–17.29).

P. Pillutla
Division of Cardiology,
Department of Medicine, Los Angeles Medical Center,
Harbor-University of California, Torrance, CA, USA
e-mail: ppillutla@labiomed.org

J.A. Aboulhosn (✉)
Ronald Reagan/UCLA Medical Center,
Ahmanson Adult Congenital Heart Disease Center,
100 Medical Plaza Drive, Suite 770, Los Angeles, CA 90095, USA
e-mail: jaboulhosn@mednet.ucla.edu

M.J. Budoff et al. (eds.), *Atlas of Cardiovascular Computed Tomography*, https://doi.org/10.1007/978-1-4471-7357-1_17

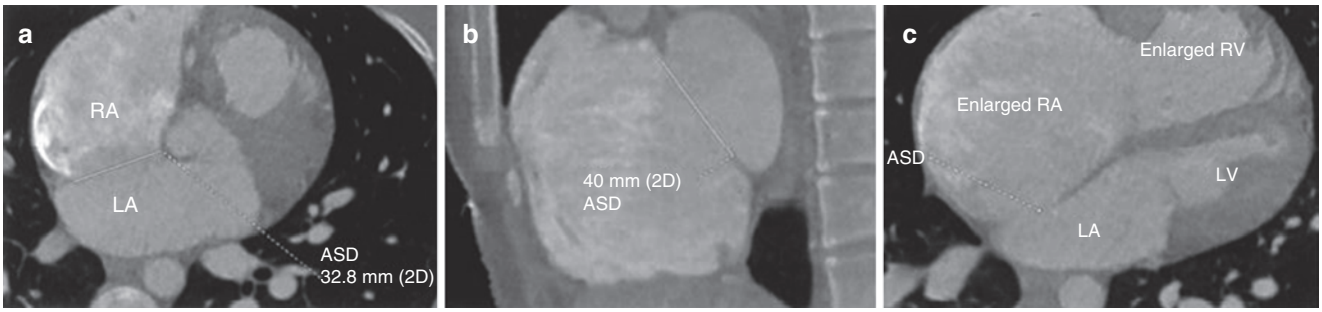

Fig. 17.1 Contrast-enhanced electron beam computed tomography (EBCT) study in an adult with an unrepaired secundum atrial septal defect (ASD) [1]. (**a**) Axial cut at the level of the maximum horizontal diameter of the ASD, which measures 33 mm; note the dilated right atrium (RA). (**b**) Sagittal cut at the level of the maximum vertical diameter of the ASD, measuring 40 mm; note the severely dilated RA. Evaluation of maximum ASD diameter in multiple planes is imperative to the proper selection of patients for percutaneous versus surgical defect closure. In this case, the patient was referred for surgical closure because the vertical diameter exceeded the maximum percutaneous device size available (38 mm). (**c**) Note the enlarged RA and right ventricle (RV), compared with the normal size of the left atrium (LA) and left ventricle (LV)

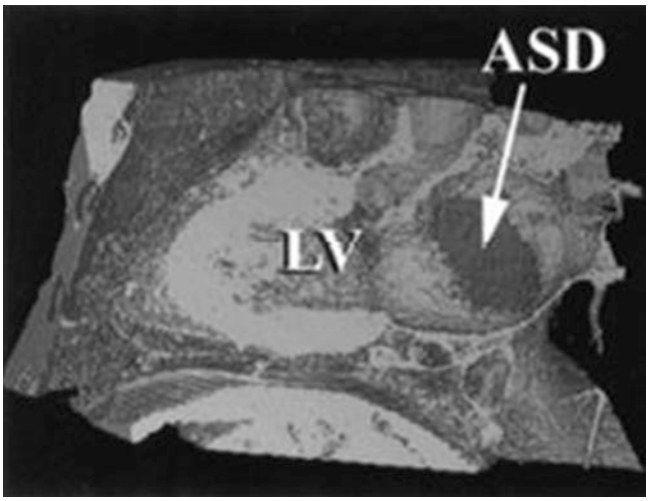

Fig. 17.2 Contrast-enhanced electron beam computed tomography (EBCT) study with three-dimensional surface rendering in a 32-year-old woman with a secundum atrial septal defect (ASD). The heart is viewed from a posterolateral and cranial projection. The posterior wall of the left atrium has been excised, as has the free wall of the left ventricle (LV). The three-dimensional geometry of this septal defect is well visualized. The defect measured 32 mm in greatest diameter. The rims are deficient in the anterosuperior (retroaortic) and posteroinferior quadrants, but are present and sufficient in all other quadrants. A 34-mm Amplatzer septal occluder (St. Jude Medical; St. Paul, MN) was used to successfully occlude this ASD

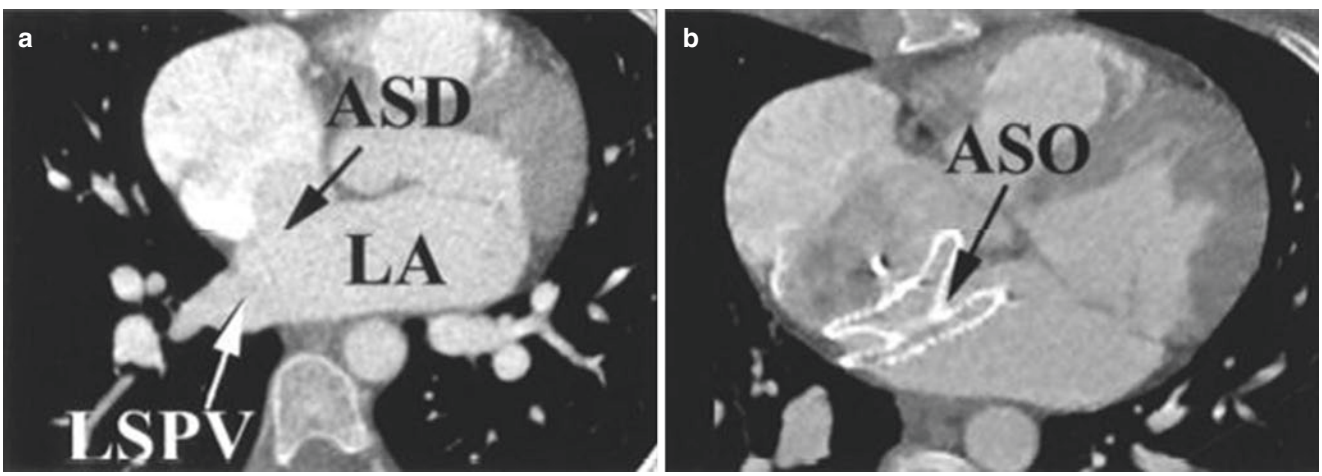

Fig. 17.3 Contrast-enhanced electron beam computed tomography (EBCT) study axial slices in a 33-year-old woman with a secundum atrial septal defect (ASD) [2]. (**a**) Prior to closure, the left superior pulmonary vein (LSPV) drains normally to the left atrium (LA). The ASD measures 34 mm in greatest horizontal diameter. (**b**) Following closure with a 38-mm Amplatzer septal occluder (ASO), the device remained in a stable position despite the virtual absence of a posterior rim

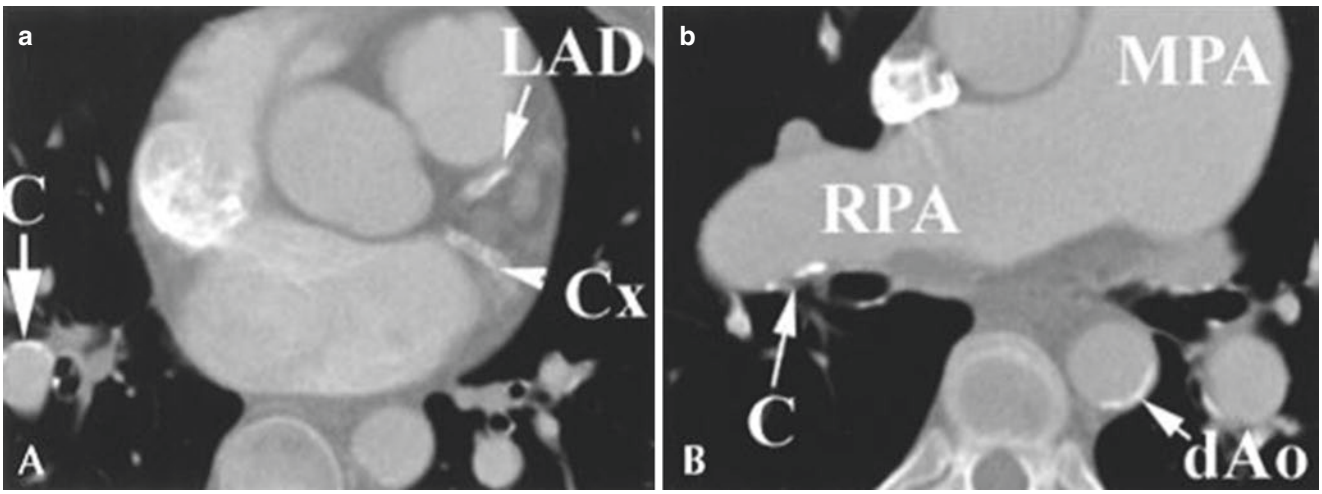

Fig. 17.4 A 16-slice CT angiogram in a 57-year-old woman with cyanosis, severe pulmonary hypertension, and an atrial septal defect. This patient had a strong family history of coronary artery disease (two brothers and her father had myocardial infarction in the third decade). (**a**) Axial slice at the level of the left coronary artery bifurcation demonstrates abundant calcium deposition in the proximal left anterior descending (LAD) and circumflex (Cx) arteries. Note the presence of calcium deposits (C) within a segmental branch of the right pulmonary artery. Pulmonary arterial calcification and atherosclerotic plaquing are present in patients with longstanding pulmonary hypertension [3]. (**b**) Axial slice at the level of a dilated main pulmonary artery (MPA) and right pulmonary artery (RPA). Note the calcium deposits within the wall of the RPA and in the descending aorta (dAo)

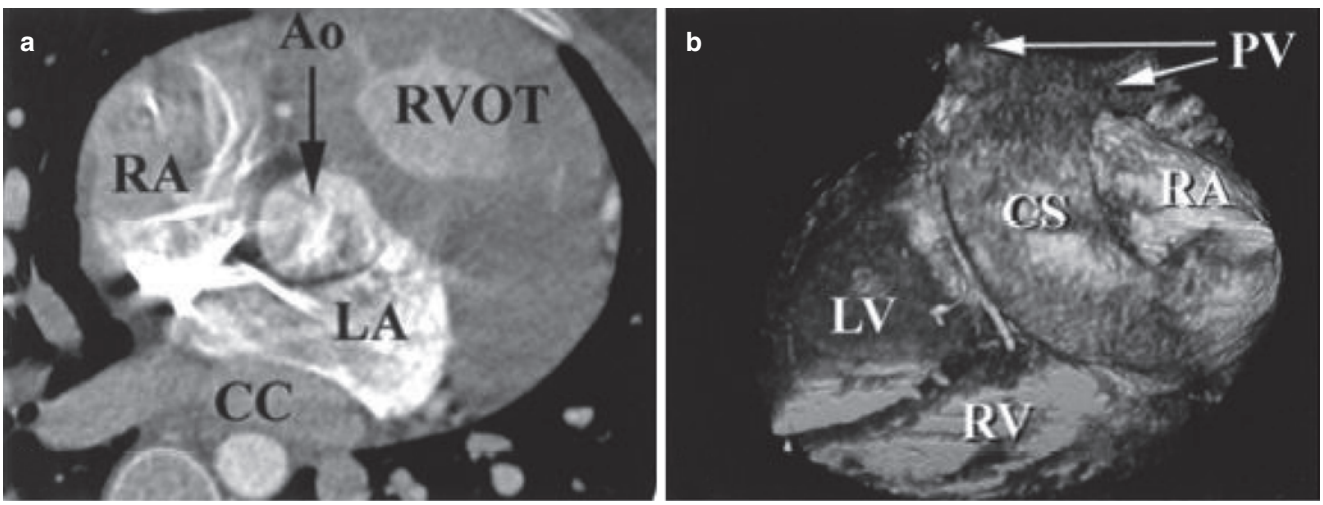

Fig. 17.5 A 64-slice CT angiogram in a 28-year-old cyanotic man with uncorrected total anomalous pulmonary venous connection (TAPVC) to the coronary sinus. (**a**) Axial cut demonstrating anomalous pulmonary venous drainage into a posterior confluence chamber (CC) that does not communicate with the left atrium (LA) or right atrium (RA). A secundum atrial septal defect (ASD) is present and allows flow to the LA. (**b**) Three-dimensional volume rendering as viewed from a posterior and caudal projection. Note the connection of the pulmonary veins (PV) to a severely dilated coronary sinus (CS), which drains into the right atrium (RA). Note the severely dilated right ventricle (RV), in contrast to the comparatively normal left ventricle (LV). Ao—ascending aorta; *RVOT*—right ventricular outflow tract

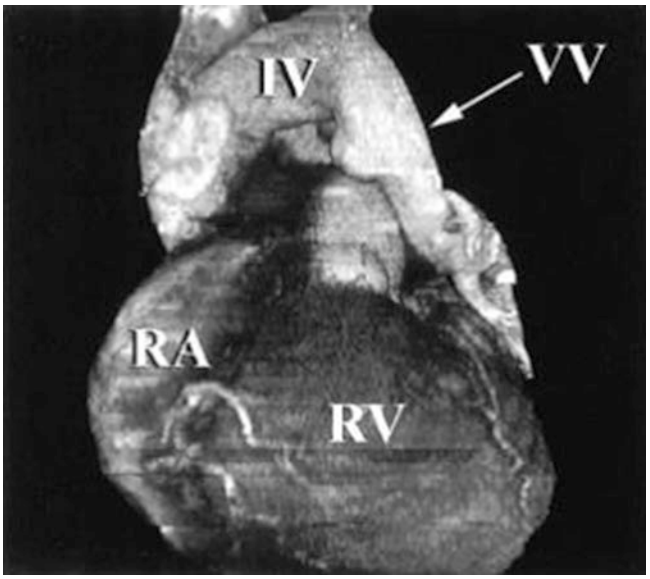

Fig. 17.6 Electron beam angiogram with three-dimensional volume rendering of a 48-year-old cyanotic woman with total anomalous pulmonary venous connection via a vertical vein (VV) to the innominate vein (IV). Note the severely dilated right atrium (RA) and right ventricle (RV)

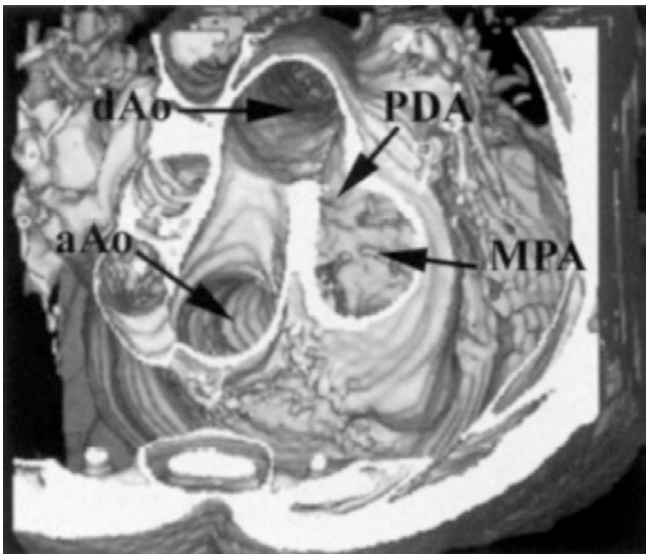

Fig. 17.8 Electron beam angiogram with three-dimensional surface rendering in a cyanotic adult with an unrepaired large patent ductus arteriosus (PDA) as viewed from a cranial projection. Note the dilated main pulmonary artery (MPA). The PDA connects the MPA to the proximal descending thoracic aorta (dAo). *aAo*—ascending aorta

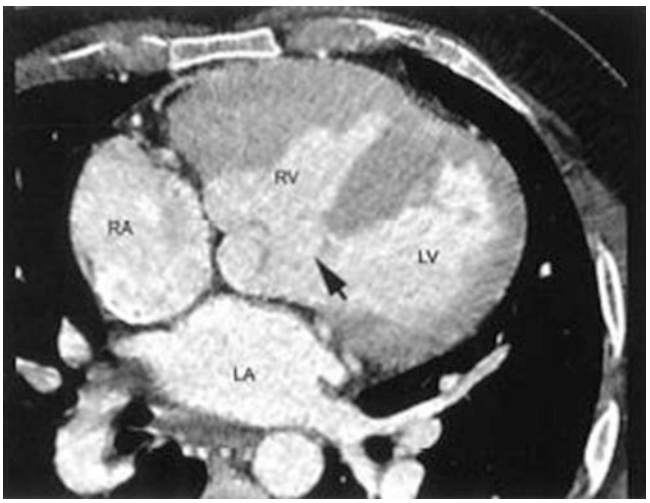

Fig. 17.7 An electron beam angiogram axial slice is shown in a 38-year-old cyanotic man with Eisenmenger's complex, characterized by a nonrestrictive, perimembranous ventricular septal defect (*arrow*) and right-to-left shunt secondary to systemic level pulmonary vascular resistance. Note the severely hypertrophied right ventricle (RV), compared with the normal left ventricle (LV). *LA*—left atrium, *RA*—right atrium

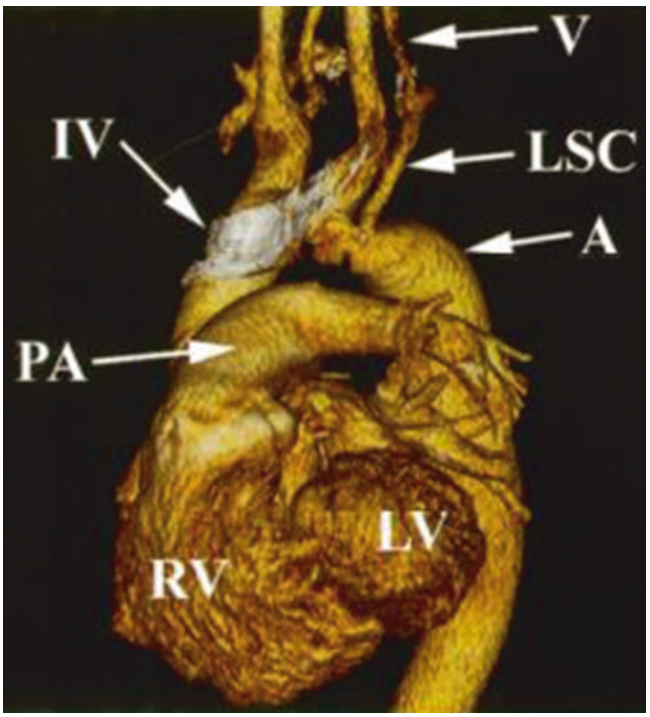

Fig. 17.9. A 64-slice CT angiogram with three-dimensional surface rendering viewed from a left anterior oblique projection. There is residual coarctation of the aorta and isthmus hypoplasia in a patient with prior surgical end-to-end repair. The post-coarctation aorta (A) is moderately dilated. The left subclavian (LSC) artery is diminutive, as is the left vertebral artery (V). *IV*—innominate vein, *LV*—left ventricle, *PA*—pulmonary artery, *RV*—right ventricle

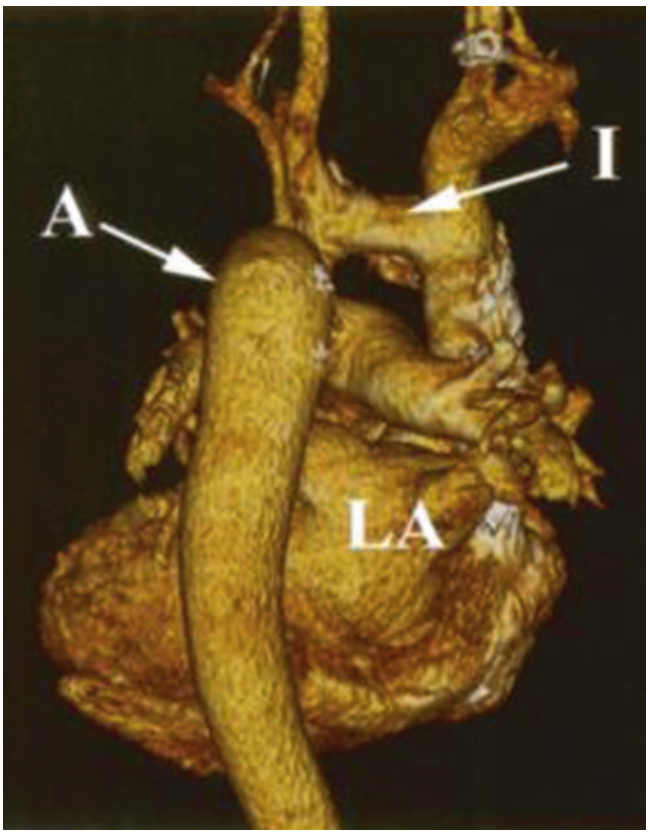

Fig. 17.10 Three-dimensional surface rendering of 64-slice CT angiography viewed from a posterior projection. There is hypoplasia of the aortic isthmus (I) in a patient with previous surgical repair (end-to-end anastomosis) of coarctation of the aorta. There is moderate residual coarctation and aneurysmal dilatation of the post-coarctation aorta (A). *LA*—left atrium

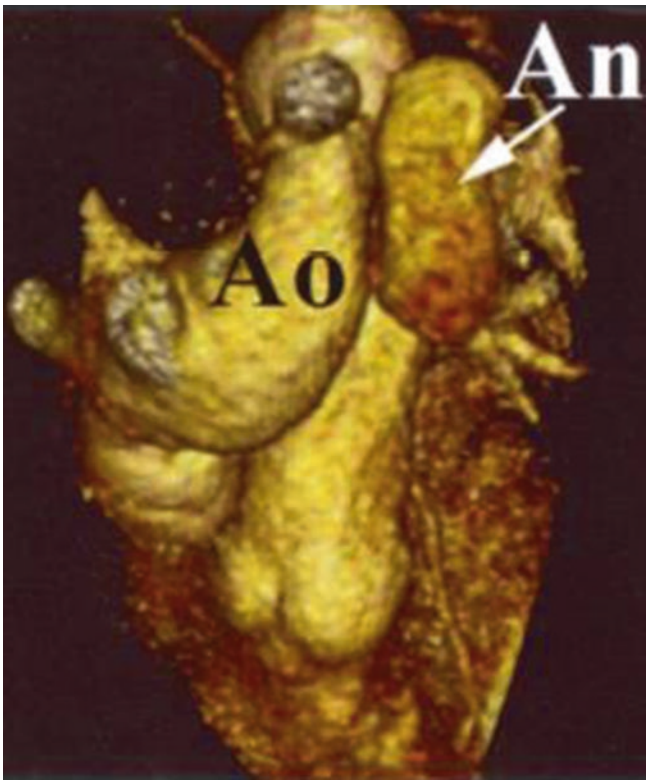

Fig. 17.11 A 64-slice CT angiogram with three-dimensional volume rendering of an adult 6 months after patch repair of coarctation of the aorta, as viewed from a left oblique and cranial angulation. Note the characteristic hypoplasia of the distal aortic arch (Ao). A large pseudoaneurysm (An) is present at the site of the previous patch aortoplasty. Aneurysm formation is a frequent complication following patch repair of aortic coarctation, leading to a decline in the use of this technique

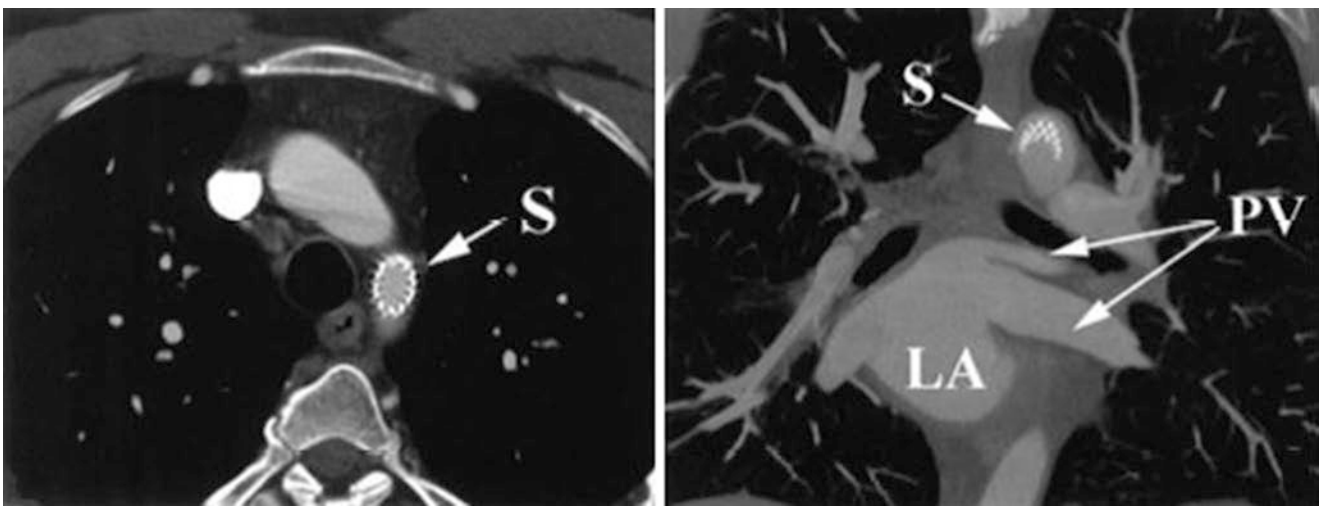

Fig. 17.12 A 64-slice CT angiogram of an adult with coarctation of the aorta following endovascular stent deployment. (**a**) An axial cut at the level of the proximal descending thoracic aorta demonstrates a widely patent, well-apposed 14-mm bare-metal uncovered stent (S) (Palmaz Genesis 2910B [Cordis Corporation, Miami Lakes, FL]). (**b**) A coronal section demonstrates the patent stent (S) in the proximal descending thoracic aorta. *LA*—left atrium, *PV*—(left superior and inferior) pulmonary veins

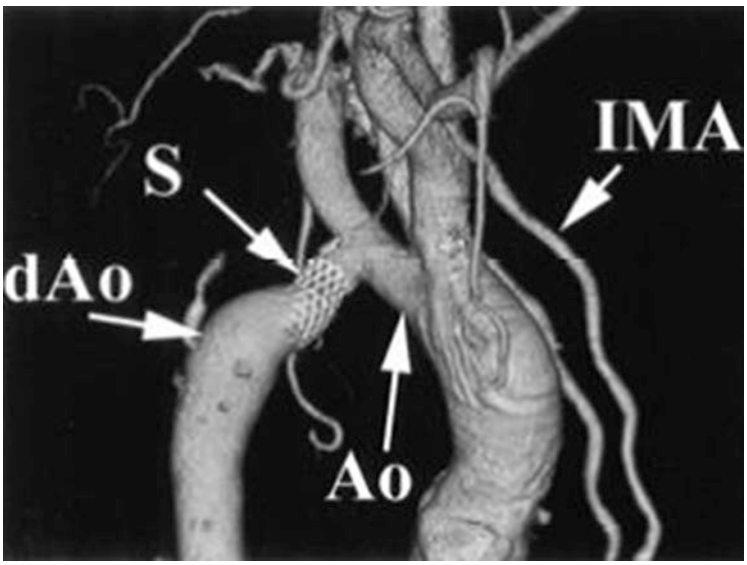

Fig. 17.13 A 64-slice CT angiogram with three-dimensional volume rendering of an adult with coarctation of the aorta following deployment of an endovascular stent (S), as viewed from a right posterior oblique projection. Note the characteristic hypoplasia of the aortic arch (Ao), the dilated post-stenotic descending thoracic aorta (dAo), and the dilated right internal mammary artery (IMA), a common finding in patients with coarctation of the aorta

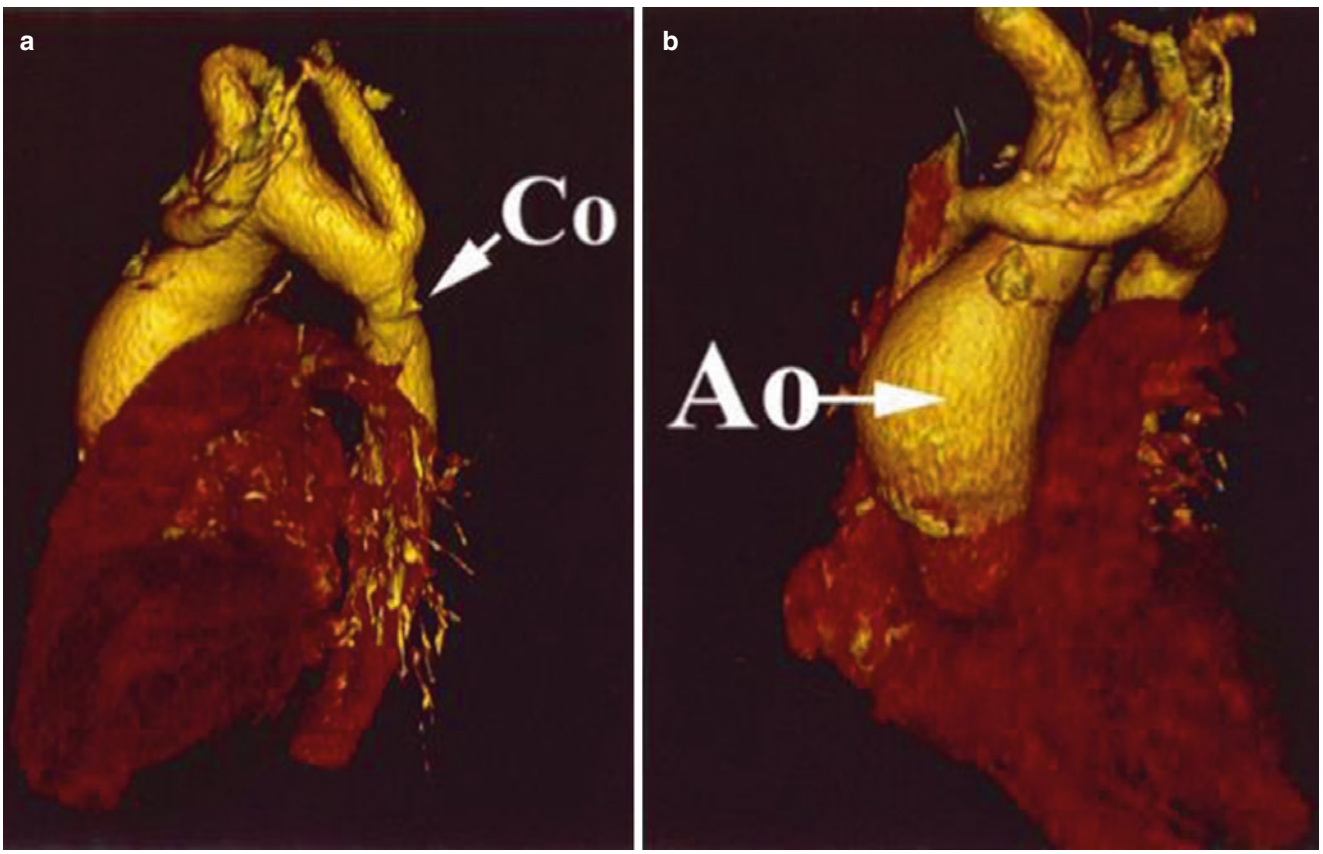

Fig. 17.14 A 64-slice CT angiogram with three-dimensional surface rendering of a 42-year-old man with coarctation of the aorta following surgical resection and end-to-end repair during childhood. The patient also has a minimally stenotic and mildly regurgitant bicuspid aortic valve. (**a**) Left anterior oblique projection demonstrating mild residual stenosis at the site of coarctation repair (Co). (**b**) Slight left anterior oblique and cranial projection demonstrating a dilated ascending aorta (Ao) measuring 50 mm in diameter above the sinotubular junction. Dilation of the aortic root in the presence of a non-stenotic or non-regurgitant aortic valve is frequently encountered and is likely related to a combination of turbulent transvalvar flow and intrinsic medial abnormalities of the aortic wall [4]

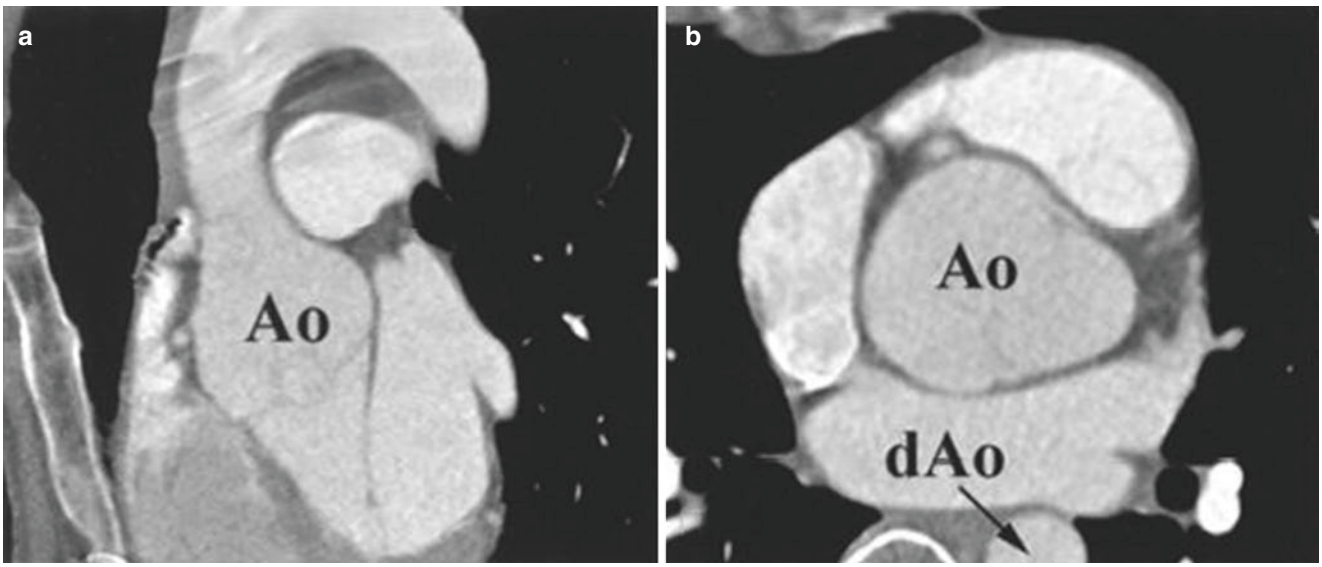

Fig. 17.15 A 64-slice CT angiogram of a 20-year-old man with Marfan syndrome. (**a**) Sagittal cut demonstrating the characteristic "Erlenmeyer flask" appearance of the aortic root (Ao). The aorta measured 53 mm at the level of the sinuses, spurring a referral for surgical aortic root repair. (**b**) Axial cut at the level of the dilated aortic sinuses (Ao). Note the stark contrast in diameter between the dilated aortic root and the normal caliber of the descending thoracic aorta (dAo)

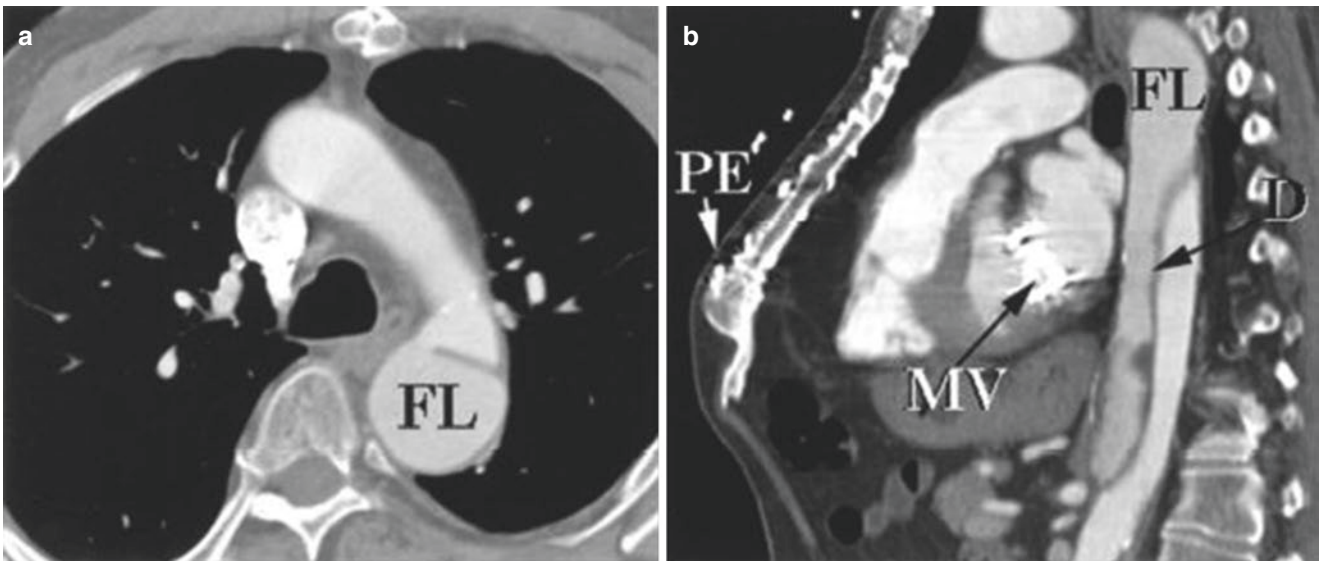

Fig. 17.16 A 16-slice CT angiogram is shown of a 61-year-old man with Marfan syndrome, a chronic Stanford type B dissection, and a mechanical mitral valve prosthesis. (**a**) Axial cut at the level of the aortic arch, demonstrating a dissection flap starting at the distal arch; FL indicates the false lumen. (**b**) Sagittal slice demonstrating pectus excavatum (PE), type B dissection (D) with a less-opacified FL, and the mechanical mitral valve prosthesis (MV)

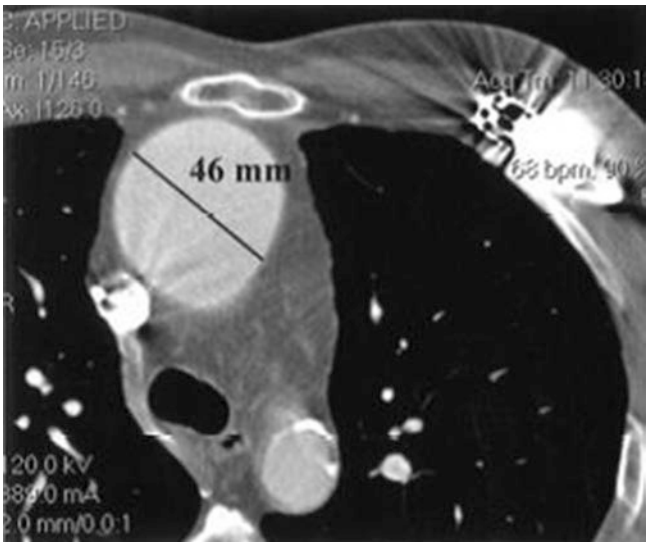

Fig. 17.17 Axial slice of a 64-slice CT angiogram in a patient with tetralogy of Fallot with pulmonary atresia, who had undergone previous intracardiac repair. Note the dilated ascending aorta, measuring 46 mm in diameter. A dilated aortic root and ascending aorta are commonly found in patients with tetralogy of Fallot and pulmonary atresia. Older age at complete repair is a risk factor for aortic root dilatation [5, 6]. This patient had a palliative shunt from infancy and underwent complete repair as a teenager

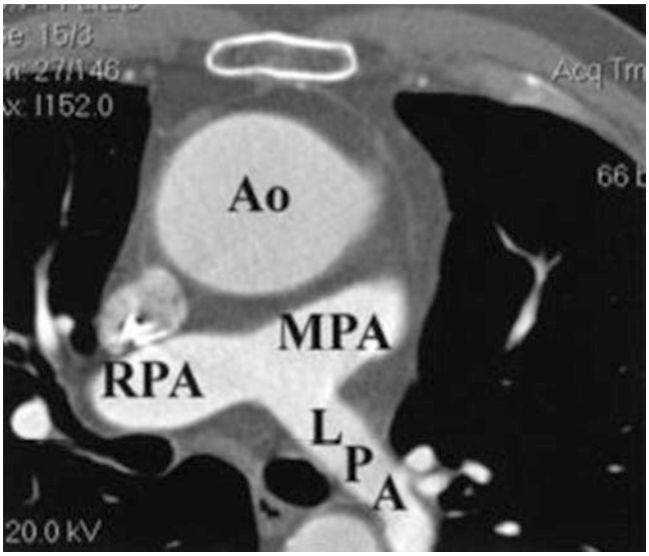

Fig. 17.18 Axial slice of a 64-slice CT angiogram in a patient with tetralogy of Fallot with pulmonary atresia, who had undergone previous intracardiac repair. Note the dilated ascending aorta (Ao). The main and branch pulmonary arteries (MPA, RPA, LPA) are small in caliber, a common finding in repaired tetralogy of Fallot with pulmonary atresia

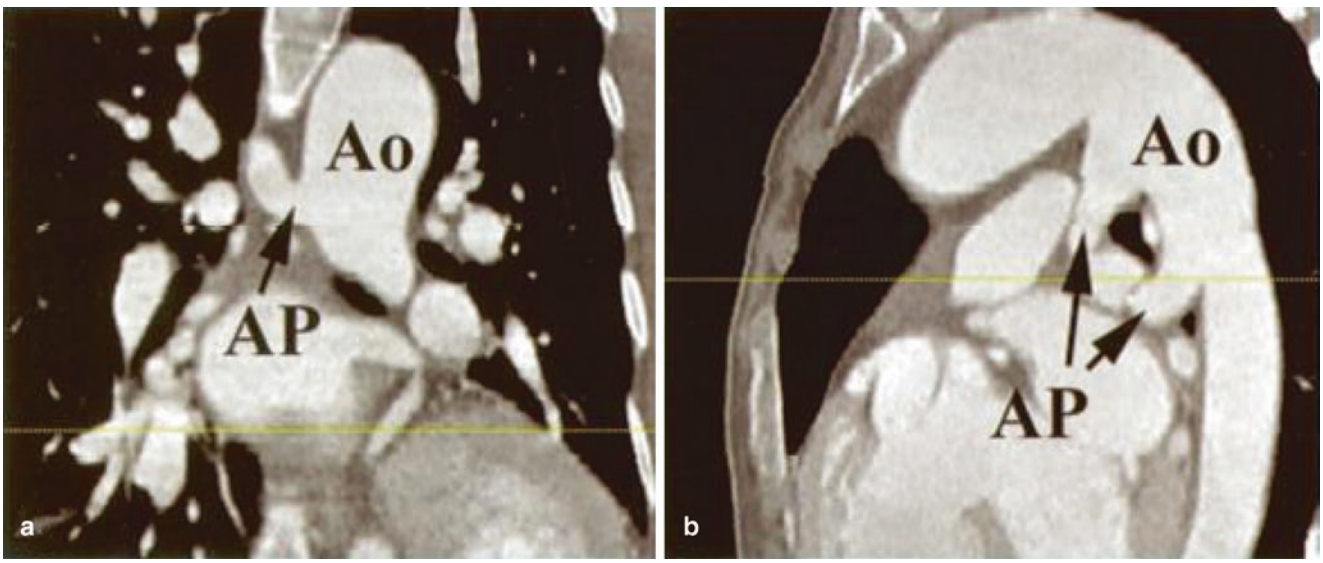

Fig. 17.19 Electron-beam angiogram of a cyanotic adult with unrepaired tetralogy of Fallot with pulmonary atresia and multiple aortopulmonary (AP) collaterals. (**a**) Coronal slice demonstrating a large AP collateral emerging rightward from the descending thoracic aorta (Ao). (**b**) Sagittal slice demonstrating two AP collaterals emerging anteriorly from the descending Ao. Delineating the origin, course, and patency of these AP collaterals is challenging and time-consuming, but it is essential for the management of these patients. Depending on the anatomic findings, patients may be candidates for complete surgical repair, unifocalization, or transcatheter interventions

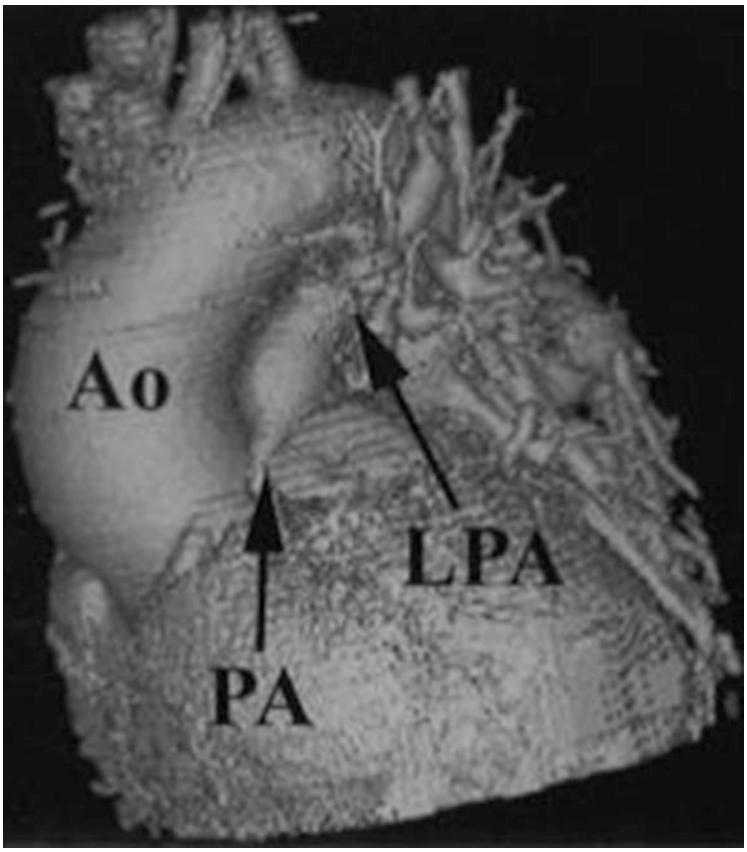

Fig. 17.20 Electron-beam angiogram with three-dimensional surface rendering of a cyanotic adult patient with unrepaired tetralogy of Fallot and pulmonary atresia, as viewed from an anterior and slightly cranial angulation. Note the dilated ascending aorta (Ao) and the atretic pulmonary artery (PA). The patient has severe stenosis/hypoplasia of the left pulmonary artery (LPA)

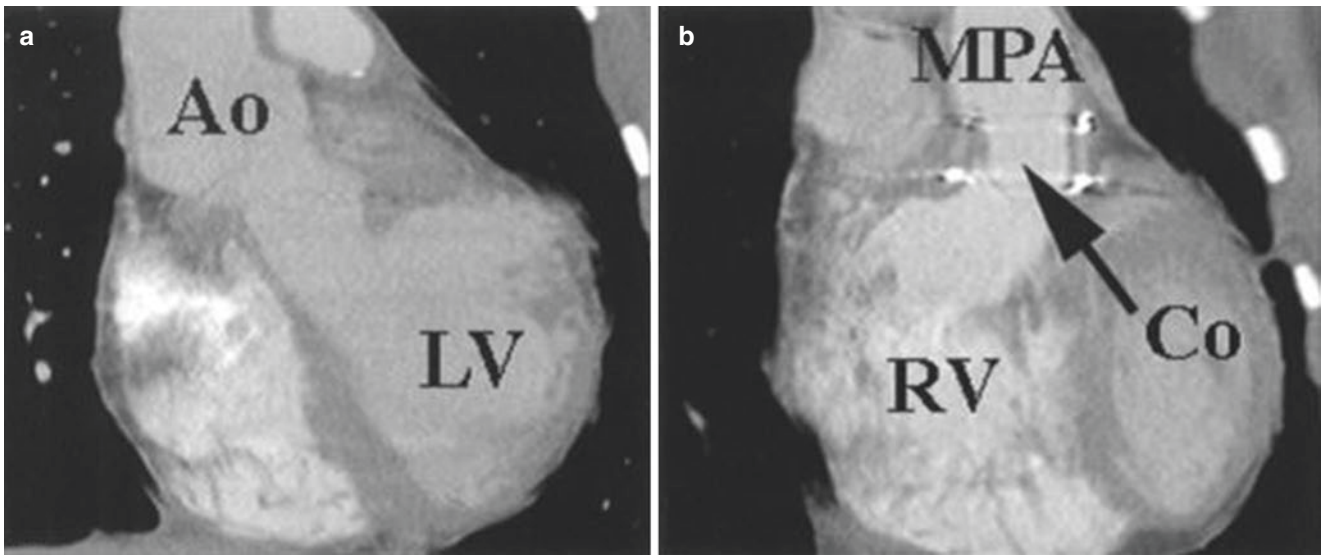

Fig. 17.21 A 64-slice CT angiogram coronal slice of a patient with a Rastelli-type surgical repair of D-transposition of the great arteries with a double-outlet right ventricle. (**a**) Patent left ventricle (LV) to aorta (Ao) internal baffle. (**b**) Right ventricle (RV) to main pulmonary artery (MPA) valved conduit (Co)

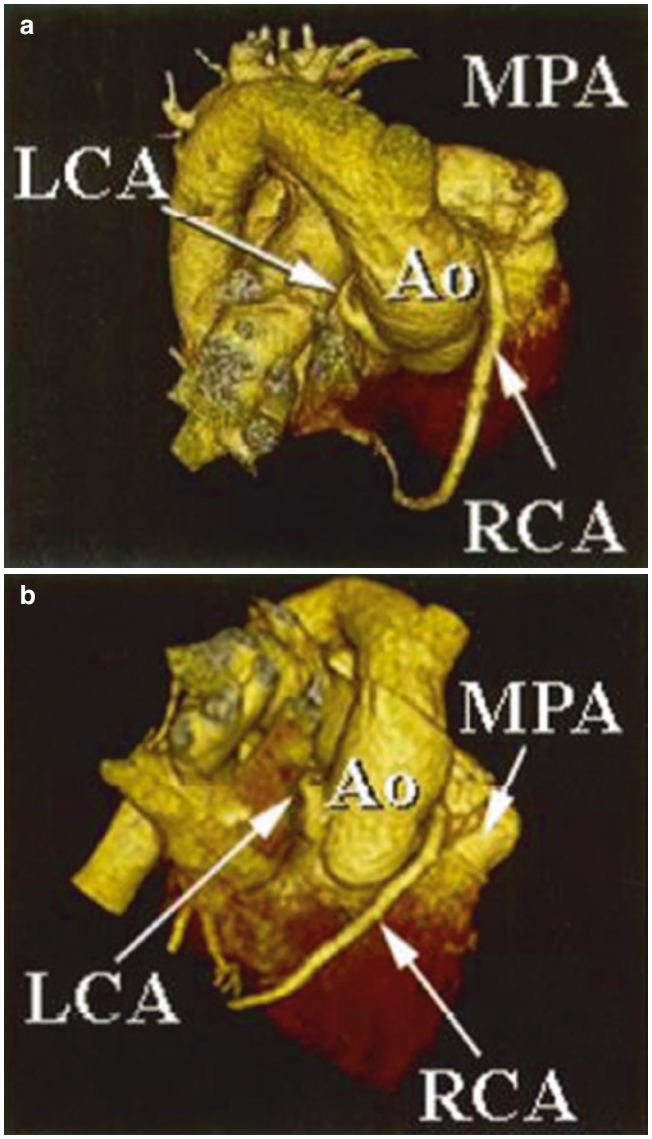

Fig. 17.22 A 16-slice CT angiogram with three-dimensional volume rendering of a 21-year-old woman with repaired tetralogy of Fallot. (**a**) In a right anterior oblique and cranial projection, the right coronary artery (RCA) emerges from the anterior and left-facing cusp and courses between the aortic root (Ao) and the main pulmonary artery (MPA). The left coronary artery (LCA) emerges from the posterior-facing cusp and courses leftward behind the Ao and below the MPA. (**b**) Right anterior oblique caudal projection

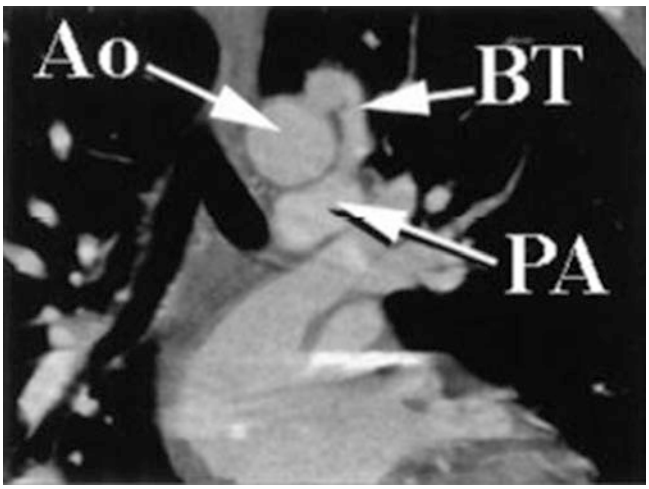

Fig. 17.23 A 64-slice CT angiogram coronal slide in a 49-year-old patient with pulmonary atresia. Note the classic left Blalock-Taussig shunt (BT) connecting the aorta (Ao) to the left pulmonary artery (PA)

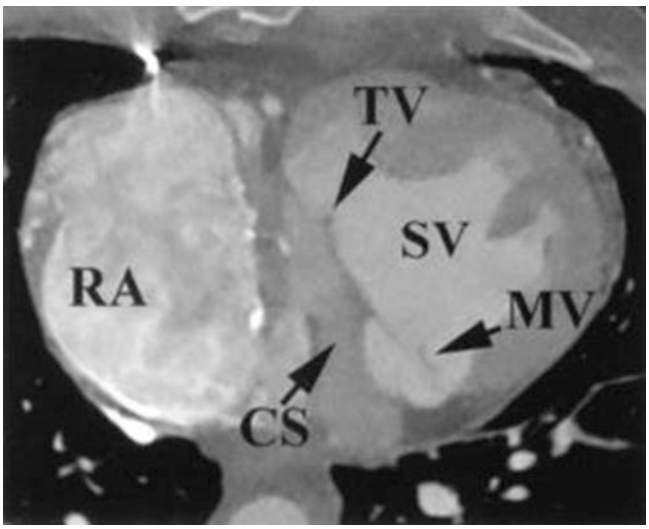

Fig. 17.24 Electron-beam angiogram (axial slice) of a 48-year-old patient with a double-inlet single ventricle after a modified right atrial to pulmonary artery (PA) Fontan operation [7]. Note the severely dilated right atrium (RA), which is a characteristic finding in patients with this form of the Fontan connection. Supraventricular arrhythmias are very common, and patients often develop signs of volume overload. This form of Fontan has been abandoned in favor of the extracardiac and lateral tunnel Fontan, but patients who underwent the Fontan operation in the 1970s and 1980s are likely to have an RA-PA connection. Simultaneous upper- and lower-extremity contrast injections are preferred for individuals with lateral tunnel or extracardiac Fontan connections as they may have preferential, asymmetric streaming from the Glenn anastomosis into one lung. Although individuals with RA-PA Fontans do not have streaming, lower extremity injections can be helpful to characterize any venous collaterals arising from the inferior vena cava or hepatic veins. Note the well-developed mitral valve (MV) and tricuspid valve (TV). The coronary sinus (CS) is well visualized and drains deoxygenated blood into the surgically created "left atrium," resulting in a right-to-left shunt and contributing to systemic hypoxia (peripheral saturation on room air of 92%). This single ventricle (SV) is of left ventricular morphology

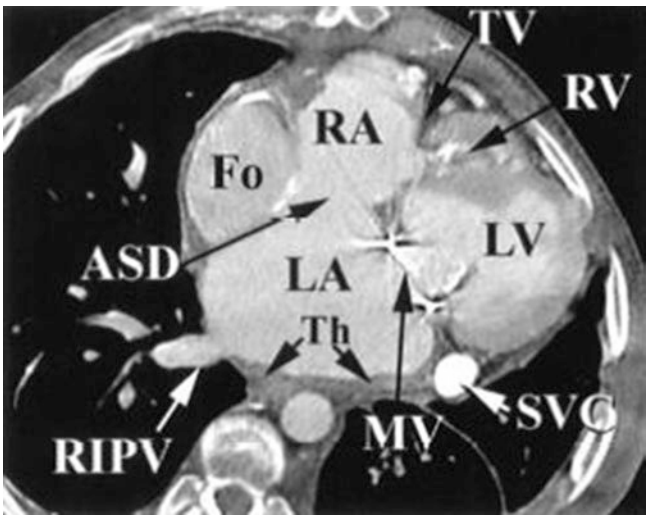

Fig. 17.25 Electron-beam angiogram (axial slice) of a 22-year-old patient with tricuspid and pulmonary atresia after a lateral tunnel Fontan (Fo) and mitral valve replacement with a mechanical prosthesis (MV). Contrast injections were performed simultaneously in the left upper extremity and the right femoral vein, resulting in opacification of the lateral tunnel Fontan and a persistent left superior vena cava (LSVC). The left atrium (LA) has a mural thrombus (Thr) overlying the posterior wall, and the left inferior pulmonary vein is occluded. A large atrial septal defect (ASD) is present between the LA and right atrium (RA). The tricuspid valve (TV) is atretic and the right ventricle (RV) is hypoplastic. The left ventricle (LV) is well developed. This case illustrates the complexity of certain types of adult congenital heart disease and how much information can be gleaned by careful analysis of the information provided by CT angiography. *RIPV*—right inferior pulmonary vein

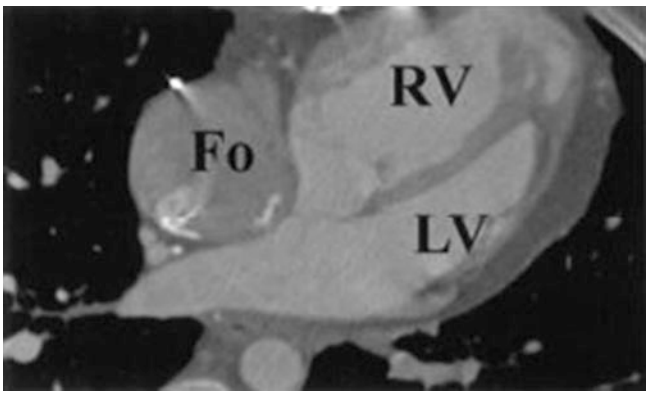

Fig. 17.26 Axial cut of a 64-slice CT angiogram in an 18-year-old patient with a hypoplastic left ventricle (LV) and a systemic right ventricle (RV) after lateral tunnel Fontan (Fo). Note the poor opacification of the Fontan after contrast injection via an upper extremity peripheral vein, a characteristic problem in these patients. Better contrast opacification of the extracardiac Fontan can be achieved if two injectors are utilized, with appropriately timed injections made in upper- and lower-extremity veins

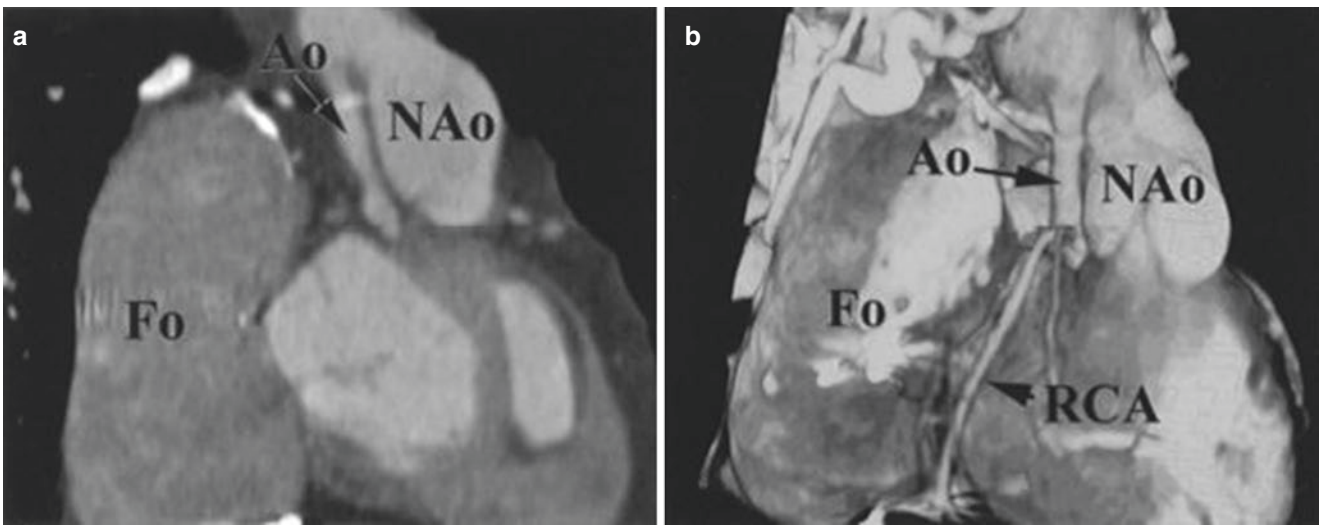

Fig. 17.27 A 64-slice CT angiogram of an 18-year-old patient with hypoplastic left heart syndrome who had successfully undergone the three stages of the Norwood operation in infancy and childhood: Stage 1. Direct anastomosis of the main pulmonary artery to the aortic arch to form a neo-aorta (NAo). The hypoplastic native ascending aorta (Ao) essentially forms a long conduit to the coronary arteries. The connection to the right coronary artery (RCA) is well seen. Pulmonary blood flow in this first stage of the Norwood operation is via a surgically placed arteriopulmonary shunt or a shunt from the right ventricle (RV) to the pulmonary artery (not shown in the figure). Stage 2. Surgical placement of a Glenn shunt (superior vena cava to right pulmonary artery) and takedown of the arteriopulmonary or RV-to-pulmonary-artery shunt. Stage 3. Surgical completion of a total cavopulmonary Fontan shunt (Fo) with alleviation of cyanosis. (**a**) Coronal slice showing the NAo and Ao as well as the lateral tunnel Fontan (Fo). (**b**), Three-dimensional volume rendering viewed from an anteroposterior and slightly cranial angulation, demonstrating the NAo, Ao, and the connection of the Ao to the RCA

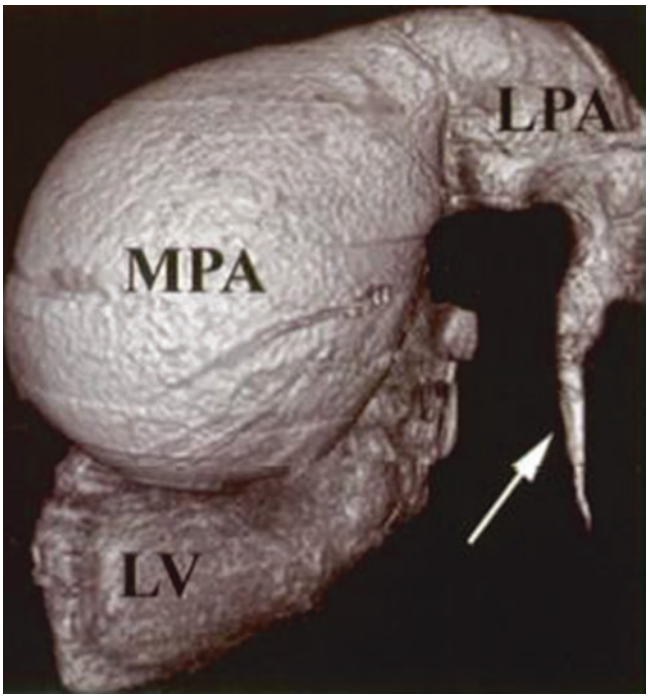

Fig. 17.28 A 64-slice CT angiogram with three-dimensional volume rendering, viewed from the lateral projection. This image shows a very large main pulmonary artery (MPA) aneurysm in a patient with severe pulmonary hypertension. This aneurysm measured 9 cm in diameter. Note the dilated left pulmonary artery (LPA) and the distal pruning of the pulmonary arterial tree (*arrow*). *LV*—left ventricle

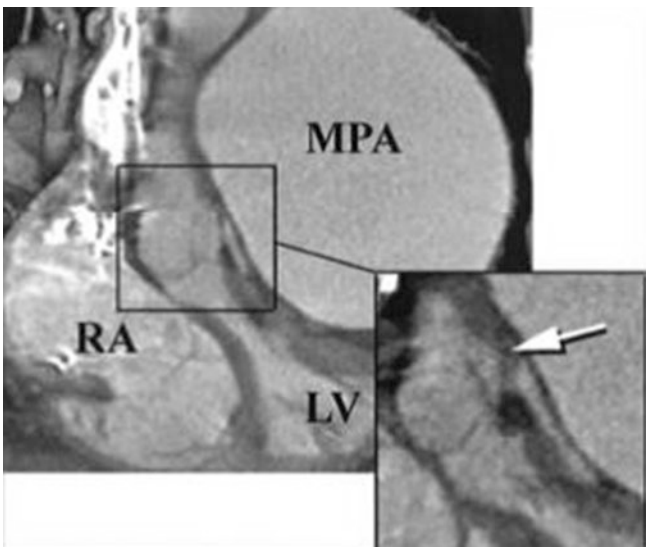

Fig. 17.29 A 64-slice CT angiogram, coronal perspective, demonstrating a large main pulmonary artery (MPA) aneurysm in a patient with pulmonary hypertension. The aneurysm compresses the left main coronary artery (*arrow*), causing a severe stenosis that results in hypotension and ischemic electrocardiographic changes. The left ventricle (LV) is small and the outflow tract is narrowed, but there was only a minimal systolic pressure gradient across this narrowed segment on invasive catheter pullback from the LV to the aorta. *RA*—right atrium

References

1. Aboulhosn J, French WJ, Buljubasic N, Matthew RV, Budoff MJ, Shavelle DM. Electron beam angiography for the evaluation of percutaneous atrial septal defect closure. Catheter Cardiovasc Interv. 2005;65:565–8.
2. Aboulhosn J, Shavelle DM, Matthews R, French WJ, Buljubasic N, Budoff MJ. Images in cardiology: electron beam angiography of percutaneous atrial septal defect closure. Clin Cardiol. 2004;27:702.
3. Aboulhosn J, Castellon YM, Siegerman C, Ratib O, Child JS. Quantification of pulmonary calcium deposits in patients with primary and secondary pulmonary hypertension using computed tomography. Abstract 90. Presented at the Western Regional Tri-Society Conference. Carmel; 3 Feb 2006.
4. Gurvitz M, Chang RK, Drant S, Allada V. Frequency of aortic root dilation in children with a bicuspid aortic valve. Am J Cardiol. 2004;94:1337–40.
5. Niwa K, Siu SC, Webb GD, Gatzoulis MA. Progressive aortic root dilation in adults late after repair of tetralogy of Fallot. Circulation. 2002;106:1374–8.
6. Mongeon FP, Gurvitz MZ, Broberg CS, Aboulhosn J, Opotowsky AR, Kay JD, et al. Aortic root dilatation in adults with surgically repaired tetralogy of Fallot: a multicenter cross-sectional study. Circulation. 2013;127:172–9.
7. Aboulhosn JA, Shavelle DM, Castellon Y, Criley JM, Plunkett M, Pelikan P, et al. Fontan operation and the single ventricle. Congenit Heart Dis. 2007;2:2–11.